

Regular article

Joining thick section aluminum to steel with suppressed FeAl intermetallic formation via friction stir dovetailing

Md. Reza-E-Rabby^a, Kenneth Ross^a, Nicole R. Overman^a, Matthew J. Olszta^a,
Martin McDonnell^b, Scott A. Whalen^{a,*}

^a Applied Materials and Processing Group, Pacific Northwest National Laboratory, 902 Battelle Blvd., Richland, WA 99352, USA

^b U.S. Army Tank Automotive Research Development and Engineering Center, 6501 E 11 Mile Road, Warren, MI 48397, USA

ARTICLE INFO

Article history:

Received 19 December 2017

Received in revised form 23 January 2018

Accepted 23 January 2018

Available online 9 February 2018

Keywords:

Friction stir dovetailing

Joining

Intermetallics

Fracture

Friction stir welding

ABSTRACT

A new solid-phase technique called friction stir dovetailing (FSD) has been developed for joining thick section aluminum to steel. In FSD, mechanical interlocks are formed at the aluminum-steel interface and are reinforced by metallurgical bonds where intermetallic growth has been uniquely suppressed. Lap shear testing shows superior strength and extension at failure compared to friction stir approaches where metallurgical bonding is the only joining mechanism. High resolution microscopy revealed the presence of a 40–70 nm interlayer having a composition of 76.4 at.% Al, 18.4 at.% Fe, and 5.2 at.% Si, suggestive of limited FeAl₃ intermetallic formation.

© 2018 Acta Materialia Inc. Published by Elsevier Ltd. All rights reserved.

Reducing the weight of commercial automobiles and military combat systems to increase energy efficiency [1], agility, and mobility [2] can be accomplished by replacing steel components with aluminum (Al). This requires the ability to join metals with vastly different material properties and has led to the investigation of numerous alternative joining techniques [3]. Joining Al to steel is particularly difficult due to large differences in material properties such as melting temperature, density, coefficient of thermal expansion, and flow stress that govern fusion and friction-based welding. In addition, a high chemical affinity with limited solubility also encourages the formation of intermetallic compounds (IMCs), which typically result in brittle failure of the joined parts [4]. The challenges for joining Al to steel are magnified when thick structures are required, such as those utilized in military combat systems and mobile structures. In light of these challenges, a new technique for joining thick section Al to steel is a much needed advancement in the field.

Friction stir welding (FSW) is a promising technology for joining Al to steel due to its ability to reduce some deleterious welding effects compared to fusion welding [5,6]; however, there are specific challenges with brittle failure modes due to uncontrolled growth of IMCs [7]. Since IMC formation almost entirely dictates Al-steel joint performance, numerous studies have been performed to reduce heat generation in the stir zone to limit IMC thickness [8–12]. These studies show

that increasing tool engagement with the steel generates higher heat input and leads to thicker, less uniform IMC formation resulting in decreased joint strength and brittle failure [13–15]. Al-steel joint strength can be enhanced by regulating the welding parameters (i.e., rotational speed, welding speed, plunge depth, forge force) to limit IMC thickness [4,9,13,14,16–22]; two studies show a joint efficiency of 77–82% [13,23], with strength being dominated by IMC thickness and phase. In other studies, the formation of IMCs is entirely avoided by forming a strictly mechanical interlock where an FSW tool is used to deform Al into features cut into the steel [24–28] to form lap, butt, and T-joint configurations. Other techniques aimed at minimizing IMC formation include multi-pass FSW [29], FSW with interlayer fillers [30–33], friction stir scribe technology [34], and localized interfacial melting [35]. Prior efforts have reported a critical IMC thickness below which the lap shear strength is maximized, depending on alloy chemistry, for Al-steel joints [36].

Although a large body of work exists for metallurgical joining of Al to steel, only a few studies report data for Al or steel thicknesses exceeding 6 mm [37–39]. This is primarily because techniques for joining thin sheets do not generally scale well for thick plates. As such, the newly developed FSD technique fills an important gap in the published literature.

In FSD, mechanical interlocks are formed between the Al and steel, which are further reinforced by metallurgical bonds created in situ during joining [40]. In this work, FSD is demonstrated for AA6061-T651 joined to Rolled Homogeneous Armor (RHA) MIL-DTL-12560 J [41] in a lap configuration. During FSD, Al is plastically deformed into dovetail grooves pre-machined on the underlying RHA surface thus forming a

* Corresponding author at: Pacific Northwest National Laboratory, 902 Battelle Boulevard, P.O. Box 999, MSIN K2-03, Richland, WA 99352, USA.

E-mail address: scott.whelen@pnnl.gov (S.A. Whalen).

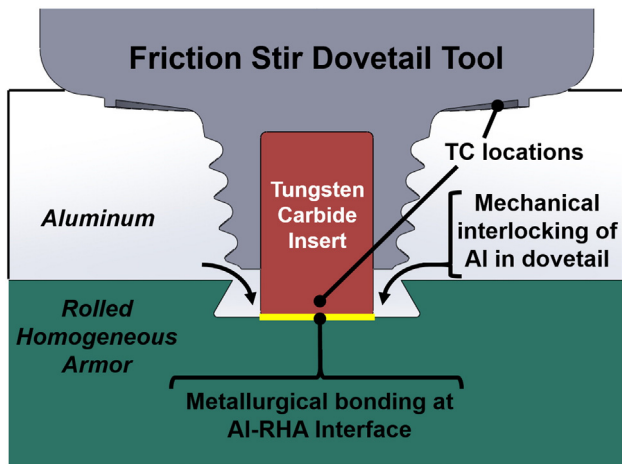


Fig. 1. Illustration of FSD technique and tooling showing mechanical interlocking and metallurgical bonding in a dovetail groove.

mechanical interlock, while engagement of a tungsten-carbide (WC) tip along the Al-RHA interface generates localized heating and results in metallurgical bonding.

Fig. 1 illustrates the FSD technique in a lap configuration with a single dovetail groove cut into the RHA. The H13 tool contains a WC insert embedded within the tool tip and type-k thermocouples are soldered at the locations indicated for the purpose of controlling temperature to limit intermetallic growth. Threads on the pin are designed to force material into the dovetail while scrolled features on the shoulder gather material to avoid formation of surface defects and interior wormholes.

RHA was cut into individual plates measuring 150 mm × 300 mm and dual disc ground to a thickness of 12.70 mm. These plates were machined with dovetail and rectangular trench grooves. Dovetail grooves had a tail width of 14.22 mm, depth of 2.54 mm, and 60° root angle along the entire 300 mm length of the RHA plate. Rectangular trench grooves had a width of 11.73 mm and depth of 2.54 mm. Al plates were machined to 150 mm × 300 mm × 12.70 mm. RHA and Al plates were then clamped in a lap configuration to the work deck of an ultra-high precision friction stir welding machine located at the Pacific Northwest National Laboratory (PNNL). FSD was performed using a tool made from H13 steel hardened to 45–48 HRC. The tool consists of a convex scrolled (3.18 mm/revolution) shoulder (38.1 mm diameter) and a frustum shaped (9°) threaded (2.12 mm/revolution) pin (15.85 mm diameter near the shank and 11 mm length) with 3 flats (120° apart). A two flatted WC insert (7.94 mm diameter) was embedded within the pin and extends 3.18 mm from the tip. Four joining trials (A, B, C, and D, as described in Table 1) were investigated to determine the impact of interlayer formation and joint configuration on lap shear strength. All trials were performed at a constant advancing speed of 76.2 mm/min. The temperature of the FSW tool was controlled to ~470 °C by dynamically modulating the spindle torque using a temperature control algorithm [42]. The tool plunge depth was controlled using a machine deflection compensation algorithm in order to regulate contact between the WC and RHA.

Table 1 summarizes the primary process parameters for the four different joining trials. For trial A, engagement between the WC insert and RHA was intentionally avoided to prevent formation of an interlayer, thereby isolating the effect of mechanical interlocking (i.e., no metallurgical bonding). For trial B, the WC tip engaged the RHA plate, without a dovetail, to isolate the effect of metallurgical bonding (i.e., no mechanical interlocking). The configuration of trial B is similar to typical Al-steel lap joint approaches found in the literature [13–15] and is used for comparison in this study. For trial C, the effects of mechanical interlocking and metallurgical bonding are combined by engaging the WC tip with the RHA along the base of the dovetail groove. Trial D is similar to trial C, except a rectangular trench is utilized rather than the dovetail geometry. The process parameters used in trials B–D were developed to limit intermetallic formation in order to reduce joint embrittlement. Tanaka et al. reported an exponential increase in joint strength as IMC thickness decreased, with IMCs <100 nm exhibiting the highest tensile strength for AA7075/mild steel FSW butt joints [4]. The commanded depth was identical for all trials B, C, and D. Due to the hard contact between WC and RHA, small machining differences in plate thickness (± 0.05 mm) caused enough variation in forge force such that a slightly different rpm was required to achieve the prescribed temperature at the tool shoulder for each trial.

The Al-RHA plates from each joining trial were sectioned perpendicular to the tool path via water jet to produce 13 mm wide lap joint specimens with a gage length of 127 mm. Room temperature lap shear tensile testing was performed on six specimens from each joining trial at an extension rate of 2.54 mm/min using a 222 kN MTS test frame. Metallographic specimens from neighboring faces were then prepared via sectioning and epoxy mounting with a final surface finish established using 0.05 μ m colloidal silica. Initial investigation of interlayer formation was performed using a JEOL 7600 field emission scanning electron microscope (SEM). A low angle backscatter electron (BSE) detector was utilized to examine the joint interfaces at various regions across the sample in low kV (5–8 kV and a small probe) mode. Utilizing low kV, BSE analysis allowed for examination of the interface such that interlayer formation could be readily observed.

Specimens for transmission and scanning transmission electron microscopy (TEM and STEM) were extracted from the joint interface using FEI 3D Quanta dual-beam focused ion beam (FIB)/SEM microscope and standard FIB lift-out and milling techniques [43,44]. TEM and STEM were performed on a JEOL ARM200F equipped with an annular dark field detector (ADF) as well as a JEOL Centurio energy dispersive spectroscopy (EDS) detector (~0.9 sR collection angle). TEM analysis of the joint interface included bright field imaging as well as collection of selected area diffraction (SAD) patterns for evaluation of crystalline structure using a 100 nm aperture. STEM characterization, ADF imaging, and EDS elemental mapping were used to examine (with high resolution) microchemical changes at the joint interface to determine the composition of any interface layers as well as chemical gradients across the interface.

SEM montages and high resolution images showing the joint cross section and Al-RHA interface are visible in Fig. 2 for all four joining trials. The joint overview images confirm that Al is fully extruded into the dovetail (trials A and C) and rectangular trench grooves (trial D). SEM micrographs in the interface overview, taken near the centerline of

Table 1
Process parameters for four different FSD joining trials.

Joining trials	Lap joint configuration	Plunge depth of WC into RHA	WC tip temperature	Tool rotational speed
	Interlock geometry: type	mm	°C	RPM
A	Dovetail: mechanical interlocking	−0.22	475	165
B	Flat interface: metallurgical bonding	0.051	460	125
C	Dovetail: interlocking + bonding	0.051	485	150
D	Trench: interlocking + bonding	0.051	480	185

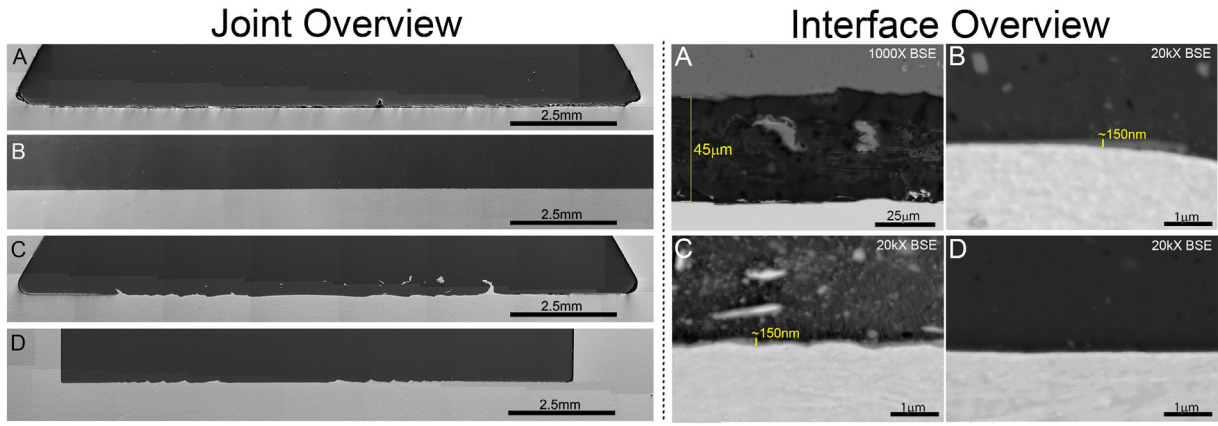


Fig. 2. Transverse section SEM montage images of the joint region for trial A–D (left) and high resolution SEM micrographs along the Al–RHA interface (right).

the Al–RHA interface, show distinct differences between the joining trials. For trial A, no metallurgical bonding is observed at the Al–RHA interface as evidenced by the ~45 μm gap between the Al and RHA. For trials B, C, and D, the SEM micrographs show a well-bonded interface with minimal interlayer formation. When present, interlayer formation for trials B and C exhibit non-uniform island-like growth with a maximum thickness of ~150 nm. The Al–RHA interfacial region of trial D shows no evidence of interlayer formation or banding of second phase dispersions. Partially formed layer structures as well as the absence of interlayer formation following friction stir joining have been reported in prior works [36,45]. For regions where a distinct interlay is not observed, closure of the mated surfaces appears to be a result of local plastic deformation at elevated temperature, which has promoted interdiffusion across the interface. Given that the WC tip temperatures were nearly identical for all joining trials, this work supports the assertion of prior studies, that contact and engagement between the FSW tooling and steel is critical to controlling formation of metallic interlayers [17], likely due to the elevated temperature exposure of clean, un-oxidized steel resulting from intense local mixing at the interface.

The effect of mechanical interlocking and interlayer formation on joint strength was characterized by lap shear tensile testing. In Fig. 3, the load-displacement curves for the four joining trials are shown

with each curve representing the average of six specimens. The y-axis shows load normalized to the thickness of each specimen (i.e., load per unit weld length) and the x-axis shows linear displacement. The macro images below the graph show the failure morphology corresponding to each of the four joining trials. In these experiments, Al was tensioned to the left and RHA to the right.

Some general observations can be made from the data in Fig. 3. Trial A has the lowest strength of the four trials and failed at the corner of the Al within the dovetail. A maximum load of 560 N/mm was observed for Trial A which compares similarly to the 470 N/mm reported in Ref [25], where mechanical interlocking is also the only joining mechanism in a thick section Al–Steel lap joint. For trial B, the maximum strength increased due to the presence of metallurgical bonding compared to trial A, but exhibited more brittle behavior with significantly lower extension at failure. For trial C, combining a dovetail interlock (trial A) with a metallurgical bond (trial B) results in a significant increase in strength and extension, with failure in the Al occurring far from the Al–RHA interface. For trial D, the groove geometry was changed to a rectangular trench and exhibited somewhat lower performance than trial C. Clearly, the combined effect of mechanical interlocking and metallurgical bonding (implemented in trials C and D) results in higher strength and greater extension at failure than metallurgical bonding alone (trial B), which is the most common approach to Al–steel friction stir welding. For trials C and D, regions where the WC insert did not contact the RHA near the groove corners are observed to pull up during lap shear testing due to a lack of metallurgical bonding. Table 2 summarizes the maximum load, extension at maximum load, and extension at fracture for the four joining trials. One standard deviation is indicated as ± in the table. Extension at fracture is defined as when the load has dropped to 70% of the maximum load. Unlike Trial B which failed by de-bonding at the Al–RHA interface, the metallurgical bond remained intact for Trials C and D and shear failure occurred within the aluminum, not at the interface, resulting in improved strength and extension. The maximum load per unit weld length mentioned in Table 2 for trials B, C, and D are 52%, 103%, and 89% above the highest known values

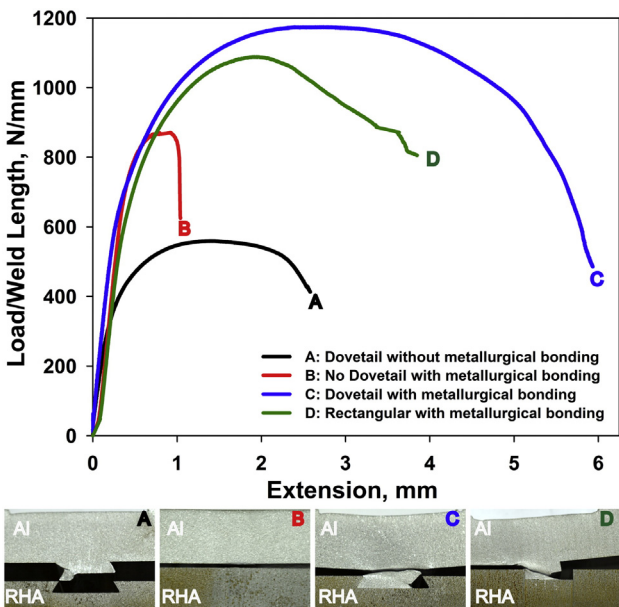


Fig. 3. Load per unit joint length vs. extension for joining trials A, B, C, and D, along with their corresponding failure morphology.

Table 2
Summary of lap shear tensile test data for joining trials A, B, C, and D.

Joining trial	Maximum interlayer thickness nm	Maximum load N/mm	Extension at maximum load mm	Extension at fracture mm
A	0	560 ± 6	1.42 ± 0.04	2.58 ± 0.05
B	~150	880 ± 23	0.83 ± 0.10	1.04 ± 0.13
C	~150	1175 ± 36	2.73 ± 0.26	5.94 ± 0.32
D	Not detected ^a	1092 ± 33	2.03 ± 0.22	3.85 ± 0.46

^a The interlayer thickness was not visible via scanning electron microscopy.

reported in the literature [35] for a lap configuration joining Al-steel by FSW.

Comparing trial B relative to trial A; the maximum load increases by 57% but the extension at fracture decreases by 60%, which is consistent with brittle metallurgical bonding. For trial C, the maximum load increases by 109% and 34% compared to trials A and B, respectively, while extension at maximum load increases by 92% and 229%, respectively. Trial D has decreased strength and extension at failure compared to trial C, suggesting that the small amount of interlocking provided by Al in the corners of the dovetail grooves contributes substantially to joint performance. IMC layers were not resolvable by SEM for trial D and the interface exhibited a sharp transition between the Al and RHA. Novel temperature control algorithms that allow for precise control of the Al-RHA interface temperature is a key development toward limiting the formation of brittle intermetallic layers in this study. The FSD approach offers the potential for improved joint strength and extension compared to typical Al-steel friction stir joints, which suffer from unregulated formation of thick IMC layers.

Due to the superior performance of trial C, a detailed TEM investigation of the interlayer was performed to better understand the structure and composition profiles present across the Al-RHA interface. Overview STEM BF images of the specimen (see Fig. 4) reveal the presence of a refined dispersion of second phase material that extends $\sim 1.5 \mu\text{m}$ into the aluminum layer from the Al-RHA interface. STEM EDS illustrates the

formation of a locally enriched Si-layer along the interface. This Si-rich layer, as measured via TEM, was found to have an average thickness of 40–70 nm. The composition of the layer was 76.4 at.% Al, 18.4 at.% Fe, and 5.2 at.% Si (63.8 wt% Al, 31.8 wt% Fe, and 4.5 wt% Si). While local silicon enrichment was observed, the Si content does not appear to cause significant embrittlement, as evidenced by the mechanical assessment.

STEM ADF imaging at elevated magnification indicates the structure of the IMC layer is polycrystalline. This observation was confirmed using SAD. Due to the refined length scale of the IMC, SAD patterns appear to incorporate through thickness diffraction from multiple grains, in addition to super-lattice reflections. This observation is in contrast to prior studies on Al-steel systems that have reported the formation of an amorphous IMC layer [38]; however, it is consistent with multiple efforts that have revealed the presence of an FeAl_3 intermetallic formation at layer thicknesses $>0.5 \mu\text{m}$ [13]. The compositional information obtained in this work suggests the interlayer formation may be an FeAl_3 intermetallic layer with local silicon enrichment.

Based on the mechanical and microstructural data, it can be concluded that FSD is a promising new technique for joining thick section Al-steel. SEM and TEM results of the Al-RHA interface have confirmed the presence of a sub-micron interlayer formation, likely FeAl_3 . The ability to inhibit the growth of IMC layers within mechanically interlocking dovetail grooves has been demonstrated. The novel tooling and temperature control approach developed herein may be used to tailor the IMC

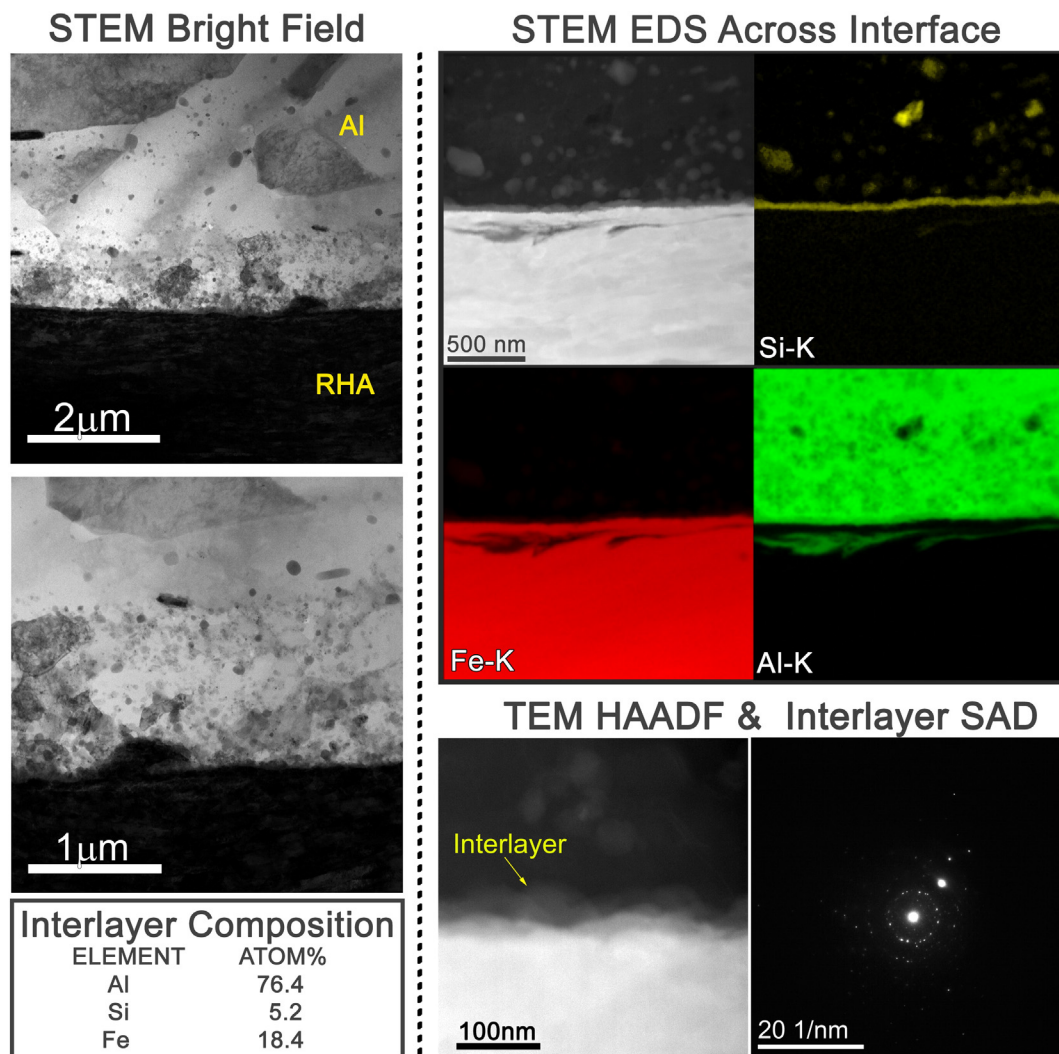


Fig. 4. STEM results obtained from the Al-RHA interface show a banded layer of refined, Si-rich, second phase dispersoids along the interface extending $\sim 1.5 \mu\text{m}$ into the Al layer. Formation of a crystalline, Si-rich intermetallic layer averaging 40–70 nm in thickness is also observed at the Al-RHA interface.

thickness in FSD or more classical FSW Al-steel joints. Joining other dissimilar materials that are otherwise unable to be welded by conventional means, such as Al-Cu, Cu-Steel, Mg-Steel, Al-Ti or metal matrix composites, may also be possible with the FSD technique.

Acknowledgements

This work was supported by the U.S. Army Tank Automotive Research, Development, and Engineering Center [Military Interdepartmental Purchase Request 10834736, 11008837, 11079043]. The Pacific Northwest National Laboratory (PNNL) is operated by the Battelle Memorial Institute for the United States Department of Energy under contract DE-AC06-76LO1830. The authors would also like to thank PNNL staff Nathan Canfield, Timothy Roosendaal, and Anthony Guzman for assisting in microstructural analysis and mechanical testing.

References

- [1] US Department of Energy, Vehicle Technologies Office, Annual Report: Lightweight Materials R&D, September 2015.
- [2] E. Polsen, L. Krogsrud, R. Carter, W. Oberle, C. Haines, A. Littlefield, Lightweight Combat Vehicle S and T Campaign US Army TARDEC/Ground System Survivability Warren United States 2014.
- [3] K. Martinsen, S. Hu, B. Carlson, CIRP Ann. Manuf. Technol. 64 (2) (2015) 679–699.
- [4] T. Tanaka, T. Morishige, T. Hirata, Scr. Mater. 61 (7) (2009) 756–759.
- [5] J. Perrett, J. Martin, P. Threadgill, M. Ahmed, 6th World Congress (Aluminium Two Thousand Conference), Florence, Italy, March 2007 13–17.
- [6] B. Thompson, K. Doherty, C. Niese, M. Eff, T. Stotler, Z. Pramann, J. Seaman, R. Spencer, P. White, Friction Stir Welding of Thick Section Aluminum for Military Vehicle Applications DTIC Document 2012.
- [7] W. Jiang, R. Kovacevic, Proc. Inst. Mech. Eng. B J. Eng. Manuf. 218 (10) (2004) 1323–1331.
- [8] C. Chen, R. Kovacevic, Int. J. Mach. Tools Manuf. 44 (11) (2004) 1205–1214.
- [9] H.A. Derazkola, H.J. Aval, M. Elyasi, Sci. Technol. Weld. Join. 20 (7) (2015) 553–562.
- [10] X. Liu, S. Lan, J. Ni, Mater. Des. 59 (2014) 50–62.
- [11] K. Ramachandran, N. Murugan, S.S. Kumar, Mater. Sci. Eng. A 639 (2015) 219–233.
- [12] A. Yazdipour, A. Heidarzadeh, J. Alloys Compd. 680 (2016) 595–603.
- [13] K. Kimpang, T. Watanabe, Mater. Trans. 46 (4) (2005) 835–841.
- [14] R.P. Mahto, R. Bhoje, S.K. Pal, H.S. Joshi, S. Das, Mater. Sci. Eng. A 652 (2016) 136–144.
- [15] Y. Wei, J. Li, J. Xiong, F. Zhang, J. Mater. Eng. Perform. 22 (10) (2013) 3005–3013.
- [16] M. Dehghani, A. Amadeh, S.A. Mousavi, Mater. Des. 49 (2013) 433–441.
- [17] A. Elrefaey, M. Gouda, M. Takahashi, K. Ikeuchi, J. Mater. Eng. Perform. 14 (1) (2005) 10–17.
- [18] M. Haghshenas, A. Abdel-Gwad, A. Omran, B. Gökçe, S. Sahraeinejad, A. Gerlich, Mater. Des. 55 (2014) 442–449.
- [19] S. Lan, X. Liu, J. Ni, Int. J. Adv. Manuf. Technol. 82 (9–12) (2016) 2183–2193.
- [20] W. Ratanathavorn, A. Melander, H. Magnusson, Sci. Technol. Weld. Join. 21 (8) (2016) 653–659.
- [21] T. Watanabe, H. Takayama, A. Yanagisawa, J. Mater. Process. Technol. 178 (1) (2006) 342–349.
- [22] R. Miller, M. McDonnell, DTIC Document, 2013.
- [23] M. Ghosh, A. Kar, K. Kumar, S. Kailas, Mater. Technol. 27 (2) (2012) 169–172.
- [24] G. Zhang, K. Zhang, J. Zhao, W. Su, J. Zhang, Patent Publication No. CN 102120287 A, Embedded Stirring and Rubbing Slit Welding Method, Xi'an Jiaotong University, 2011.
- [25] W.T. Evans, B.T. Gibson, J.T. Reynolds, A.M. Strauss, G.E. Cook, Manuf. Lett. 5 (2015) 25–28.
- [26] W.T. Evans, G.E. Cook, A.M. Strauss, in: Y. Hovanski, R. Mishra, Y. Sato, P. Upadhyay, D. Yan (Eds.), Friction Stir Welding and Processing IX, The Minerals, Metals & Materials Series, Springer, Cham 2017, pp. 79–89.
- [27] A.W. Jarrell, A.M. Strauss, G.E. Cook, in: Y. Hovanski, R. Mishra, Y. Sato, P. Upadhyay, D. Yan (Eds.), Friction Stir Welding and Processing IX, The Minerals, Metals & Materials Series, Springer, Cham 2017, pp. 91–96.
- [28] R.J. Utter, R.D. Fleck, R.J. Steel, WO Patent Publication No. 2016/007773 A1, Friction Stir Extrusion of Nonweldable Materials for Downhole Tools, Megastir Technologies LLC, 2016.
- [29] C. Leita, E. Arruti, E. Aldanondo, D. Rodrigues, Mater. Des. 106 (2016) 153–160.
- [30] Y. Chen, K. Nakata, Metall. Mater. Trans. A 39 (8) (2008) 1985–1992.
- [31] H. Das, R. Ghosh, T. Pal, Metall. Mater. Trans. A 45 (11) (2014) 5098–5106.
- [32] G. Zhang, W. Su, J. Zhang, Z. Wei, Metall. Mater. Trans. A 42 (9) (2011) 2850–2861.
- [33] Q. Zheng, X. Feng, Y. Shen, G. Huang, P. Zhao, J. Alloys Compd. 686 (2016) 693–701.
- [34] Y. Hovanski, P. Upadhyay, S. Kleinbaum, B. Carlson, E. Boettcher, R. Ruokolainen, JOM (2017) 1–5.
- [35] C. van der Rest, P.J. Jacques, A. Simar, Scr. Mater. 77 (2014) 25–28.
- [36] H. Springer, A. Kostka, J. Dos Santos, D. Raabe, Mater. Sci. Eng. A 528 (13) (2011) 4630–4642.
- [37] T. Nishida, T. Ogura, H. Nishida, M. Fujimoto, M. Takahashi, A. Hirose, Sci. Technol. Weld. Join. 19 (7) (2014) 609–616.
- [38] T. Ogura, Y. Saito, T. Nishida, H. Nishida, T. Yoshida, N. Omichi, M. Fujimoto, A. Hirose, Scr. Mater. 66 (8) (2012) 531–534.
- [39] E.E. Patterson, Y. Hovanski, D.P. Field, Metall. Mater. Trans. A 47 (6) (2016) 2815–2829.
- [40] K. Ross, Scott Whalen, Md Reza-E-Rabby, Yuri Hovanski, US Patent Application No. 15/694,565, Systems and Process for Joining Dissimilar Materials and Solid-State Interlocking Joint with Intermetallic Interface Formed Thereby, Battelle Memorial Institute, 2017.
- [41] U.S. Army Research Laboratory, Weapon and Materials Research Directorate, Materials and Manufacturing Technology Branch, MIL-DTL-12560K(MR), Armor Plate, Steel, Wrought, Homogeneous (For use in Combat-Vehicles and for Ammunition Testing), Specifications and Standards Office, Aberdeen Proving Ground, MD, 7 Dec. 2013.
- [42] K. Ross, C. Sorensen, Friction Stir Welding and Processing VII, Springer, 2013 301–310.
- [43] J. Mayer, L.A. Giannuzzi, T. Kamino, J. Michael, MRS Bull. 32 (5) (2007) 400–407.
- [44] K. Thompson, D. Lawrence, D. Larson, J. Olson, T. Kelly, B. Gorman, Ultramicroscopy 107 (2) (2007) 131–139.
- [45] R. Marstatt, M. Krutzlinger, J. Luderschmid, M. Zaeh, F. Haider, IOP Conference Series: Materials Science and Engineering, IOP Publishing, 2017 (p. 012002).